Composites Part B 233 (2022) 109648

Contents lists available at ScienceDirect

Composites Part B

journal homepage: www.elsevier.com/locate/compositesb

Delivery of mRNA vaccines and anti-PDL1 siRNA through non-invasive transcutaneous route effectively inhibits tumor growth

Kaili Wang [a], Xiaoyun Wang [b], Di Jiang [a], Yifei Pei [a], Zhe Wang [a], Xiaojun Zhou [a], Jinglei Wu [a], Xiumei Mo [a], Hongsheng Wang [a,*]

[a] Shanghai Engineering Research Center of Nano-Biomaterials and Regenerative Medicine, Key Laboratory of Science & Technology of Eco-Textile (Ministry of Education), College of Chemistry, Chemical Engineering and Biotechnology, Donghua University, Shanghai, 201620, PR China
[b] Department of Obstetrics & Gynecology, Shanghai First People's Hospital Affiliated to Shanghai JiaoTong University, Shanghai, 201620, PR China

ARTICLE INFO

Keywords:
Transcutaneous immunization
mRNA vaccines
Immune checkpoint blocker
Ethosome
Dendritic cells
Tumor immunotherapy

ABSTRACT

This study aimed to deliver mRNA vaccines and immune checkpoint blockers (ICB) with a transcutaneous immunization (TCI) system based on ethosomes (ETH), exploring the feasibility and effectiveness of their use in tumor treatment. Our data showed that the mannosylated-chitosan-modified ETH (ETH^{MC}) loaded with mRNA can efficiently transfect dendritic cells (DCs) and induce them maturation. The transdermal patches loaded with mRNA vaccines (termed TCIP) or siRNA against PDL1 (termed TDSP) were prepared by electrospraying microspheres containing mRNA- or siRNA-loaded ETH^{MC} onto the surface of silk fibroin matrices (SFM). The patches showed a good transdermal performance and can effectively deliver nucleic acid molecules into the deep layers of skin. In vivo experiments showed that TCIP loaded with mRNA vaccines can effectively trigger cellular and humoral immune responses. Using mouse melanoma as a model, the combined treatment with TCIP and TDSP showed good antitumor effect, significantly inhibiting tumor growth by improving the infiltration of $CD4^+$ and $CD8^+$ T cells as well as the apoptosis rates in tumor tissues. Our work provides a new strategy for tumor treatment by integrating the non-invasive and convenient of TCI and the flexibility of RNA therapy.

1. Introduction

Transcutaneous immunization (TCI) is a simple and relatively new method of vaccination that the antigen and adjuvants is applied onto the skin to induce systemic immune responses [1]. Dendritic cells (DCs), fibroblasts, T cells, B cells and the skin draining lymph nodes constitute the skin immune network [2]. An effective immune response can be activated when the antigen is delivered to the langerhans cells (LCs, which belong to immature DCs) in the epidermis via transcutaneous route [3]. The epidermis and dermis are rich in LCs and DCs, which makes the skin an attractive site for vaccination [4]. TCI simplify the vaccination process without the pain and the risk of infection caused by inject, thus, the coverage and safety of vaccination can be greatly improved. Besides, the transdermal delivery avoids the premature metabolism of the drug, which leads to better bioavailability [5]. Therefore, TCI represents an encouraging alternative to traditional vaccination approach.

Various TCI systems have been developed and investigated, including microneedle, lipid-based vesicles, hydrophilic gel patches, hyaluronic acid conjugates, natural polymeric nanocapsules, etc. [6]. The application of TCI systems has been extensively explored in recent years and shown promising potentials in the field of antitumor [7–14]. Among them, the most concerned one is microneedle-based TCI systems for their highly efficient at transdermal drug delivery [8–12]. Although the microneedles are much thinner than traditional needles, they can still cause minor damage to the skin and may lead to potential risk of infection. Ethosome (ETH), a special liposome containing low molecular weight alcohol, can be obtained through facile process and has good stability, high encapsulation efficiency and good performance in transdermal drug delivery without any damage to the skin [15]. By modification with galactose or mannose groups on its surface, the ETH can obtain the ability to target DCs [16–18]. DCs-targeted cationic ETHs have been proved to be useful carriers for TCI, as they can effectively trigger immune response by percutaneously delivering antigen to DCs [16–18]. TCI systems based on DCs-targeted ETHs have been reported with good antitumor effect when tumor-associated antigens or

* Corresponding author.
E-mail address: whs@dhu.edu.cn (H. Wang).

https://doi.org/10.1016/j.compositesb.2022.109648
Received 20 November 2021; Received in revised form 31 December 2021; Accepted 11 January 2022
Available online 13 January 2022

immunotherapy cytokines were encapsulated in the ETHs [16–18]. Furthermore, our recent work demonstrated that the combination therapy with ETH-based TCI and anti-programmed cell death-1 (PD1) monoclonal antibody (aPD1) could produce a synergistic anti-tumor effect [19]. The PD1 ligand 1 (PDL1) interacts with PD1 and result in inhibition of the anti-tumor response [20–22]. Antagonists against PDL1 may be safer compared with those against PD1, as PDL1 is expressed on tumor cells and DCs while PD1 is only expressed on T cells [23]. Studies have proven the advantages of knocking down PDL1 with siRNA against PDL1 (siRNA$_{Pdl1}$) in tumor immunotherapy, and DCs are a unique and important target of PDL1 blocking [24]. Considering its unique non-invasiveness and convenience, the combination of ETH-based TCI and transdermal delivery of siRNA$_{Pdl1}$ may be a promising solution for tumor treatment.

In recent years, RNA therapy represented by mRNA and siRNA have attracted much attention due to the following unique advantages: no potential risk of harmful genomic integration since mRNA needs only to be translated into protein in the cytoplasm; great flexibility in terms of production, as different products can be produced using the same established production process without adjusting the original route; half-life of mRNA *in vivo* can be adjusted by using different modifications and delivery methods [25,26]. These advantages make RNA therapy a promising prospect in the treatment of infectious diseases and tumor [27]. Tumor specific antigen-encoded mRNA can trigger antitumor immune response to kill tumor cells, many studies have reported applying mRNA vaccines to tumor immunotherapy and achieved good results [28]. However, mRNA is vulnerable to degradation by ubiquitous nucleases during the process of delivery. Currently, the most commonly used method is to encapsulate mRNA in cationic lipid nanoparticles, coupled with modification and optimization in coding and non-coding regions to increase the stability and translation efficiency of mRNA [29]. Hence, we speculate that transdermal administration of mRNA vaccines and siRNA$_{Pdl1}$ could be a useful strategy for the prevention and treatment of tumors.

Compared with creams and suspensions, patches have the advantages of convenient storage, transportation and use, and are more suitable for transdermal drug delivery (TDD). The base substrate used to construct the TDD patches must have good skin affinity. Silk fibroin (SF) from silkworm cocoon has excellent biocompatibility and is widely used in biomedical field [30–35]. SF fibrous matrices (SFM) was used as substrate to construct TDD systems in our previous studies wherein drug-loaded ETHs were distributed evenly on the SF fibers through electrospinning [32,36,37]. However, the electrospun SFM (eSFM) has poor mechanical properties and less ETH loading limited by the electrospinning itself. A feasible solution for overcoming these disadvantages is to spray microspheres containing drug-loaded ETH onto the substrates with a better mechanical performance using electrospray as reported previously, wherein polyvinylpyrrolidone (PVP) was used to form the microspheres [19,36]. PVP is a biodegradable synthetic polymer with good biocompatibility [38]. The water-soluble property of PVP is conducive to the rapid release of ETH from the microspheres and contact with the skin [19,36]. The SFM obtained by soaking (sSFM) with a $CaCl_2$-ethanol-H_2O ternary solution has been reported with good mechanical performance [39]. In addition, the ternary solution immersion method is much simpler than electrospinning. Thus, the combination of sSFM and microspheres composed of antigen-loaded ETH and PVP could be a useful strategy for the construction of TCI patches (TCIP).

In this study, we aimed to develop a novel TCIP loading mRNA vaccines based on the mannosylated-chitosan (MC) modified ETH (ETH^{MC}) and sSFM. The tyrosinase-related protein 2 (TRP2) was used as a model of tumor associated antigen, and oligodeoxynucleotides containing unmethylated CpG motifs (CpGs) as adjuvants. The mRNA of TRP2 (termed mRNA$_{Trp2}$) and CpGs were encapsulated into ETH^{MC} (termed mRNA$_{Trp2}$@ETH^{MC} and CpGs@ETH^{MC}, respectively) and then sprayed onto the sSFM by electrospray to obtain the TCIP. While the patches for transdermal delivery of siRNA$_{Pdl1}$ (termed TDSP) were obtained by electrospraying the siRNA$_{Pdl1}$-loaded ETHs (siRNA$_{Pdl1}$@ETH^{MC}) onto the sSFM. After physicochemical and biological characterization in vitro, the antitumor effect of TCIP combined with TDSP was evaluated using a syngeneic mouse model for melanoma by subcutaneous injection of B16F10 cell lines.

2. Materials and methods

2.1. Materials

Cholesterol, lecithin, octylamine, HA, chitosan (C), D-mannose (M), PVP, dimethyl sulfoxide, 4,6-diamino-2-phenylindole dihydrochloride (DAPI), fluorescein isothiocyanate (FITC), lipopolysaccharide (LPS) and 1,1′-dioctadecyl-3,3,3′,3′-tetramethylindocarbocyanine perchlorate (DiI) were purchased from Sigma-Aldrich (St Louis, MO, USA). Diethypyrocarbonate (DEPC) was purchased by Shanghai Yuanye Biology Science and Technology Co., Ltd. (Shanghai, China). Calcium chloride ($CaCl_2$) was from Shanghai Titan Technology Co., Ltd. (Shanghai, China). Three acetoxyl group sodium borohydride ($NaBH(OAc)_3$) was purchased from Yien Biotechnology Co., Ltd. (Shanghai, China). Plasmids (pcDNA™3.1(+) and pLVX-shRNA2) were purchased from Anhui General Biological Co., Ltd. (Chuzhou, China). HiScribe T7 ARCA mRNA kit was purchased from Biotechnology International Trade (Shanghai) Co., Ltd. (Shanghai, China). The cell line was purchased from Hunan Fenghui Biological Technology Co., Ltd. (Changsha, China). Cell Counting Kit-8 (CCK-8), calcein-AM/propidium iodide (PI) double stain kit, bulk plasmid extraction kit, SanPrep Column PCR product purification kit and Hoechst 33342 were purchased from Shanghai Shenggong Biology Engineering Co., Ltd. (Shanghai, China). Mulberry silkworm cocoons were purchased from Huzhou Silk Company (Huzhou, China). Phycoerythrin-labelled goat anti-mouse monoclonal antibodies of CD80 (clone No.16-10A1) and CD86 (clone No. A17199H) were from Pepro-Tech (Rocky Hill, NJ, USA). Rabbit anti-mouse CD4 (#GB13064-2) and CD8 (#GB13429) were purchased from Servilcebio Co., Ltd. (Wuhan, China). TMB enzyme-linked immunosorbent assay (ELISA) kits (IL-12, TNF-α, IFN-γ and TRP2 antibody) were purchased from Shanghai Hengyuan Biology Science and Technology Co., Ltd. (Shanghai, China). Real-time fluorescence quantitative polymerase chain reaction (PCR) kits were purchased from Nanjing Vazyme Biotech Co., Ltd. (Nanjing, China). C57BL/6 mice were purchased from Shanghai Jiesijie Experimental Animal Co., Ltd. (Shanghai, China).

2.2. Preparation of in vitro transcribed mRNA (IVT mRNA)

DNA template for the preparation of the IVT mRNA of mouse TRP2 including T7 promoter, 5′ un-translated region (UTR), open reading frame (ORF), and 3′UTR was designed and constructed into pcDNA™3.1 (+) plasmid (Fig. 1A & Table S1). Subsequently, the linearized DNA template for IVT mRNA of TRP2 (termed DNA$_{Trp2}$) was obtained by PCR. The linearized DNA template for IVT mRNA of green fluorescent protein (EGFP) (termed DNA*egfp*) was also obtained using pLVX-shRNA2 as template. The sequences of the primers were shown in Table S1. The PCR products were then purified by kit and used as templates to produce IVT mRNAs contaning 7-methyl guanosine (m7G) cap at the 5′ end and a poly(A) tail at the 3′ end with a HiScribe T7 ARCA mRNA Kit (with tailing) following the instructions of the manufacturer. The IVT mRNA products (termed mRNA$_{egfp}$ and mRNA$_{Trp2}$ for *egfp* and *Trp2*, respectively) were verified through 1% agarose gel electrophoresis and then stored at −80 °C for later use.

2.3. Preparation and characterization of ETH^{MC}

2.3.1. Synthesis of mannosylated chitosan (MC)

MC was synthesized according to a previously reported method [17]. Briefly, 2.0 mg/mL chitosan solution was prepared using 1% acetic acid

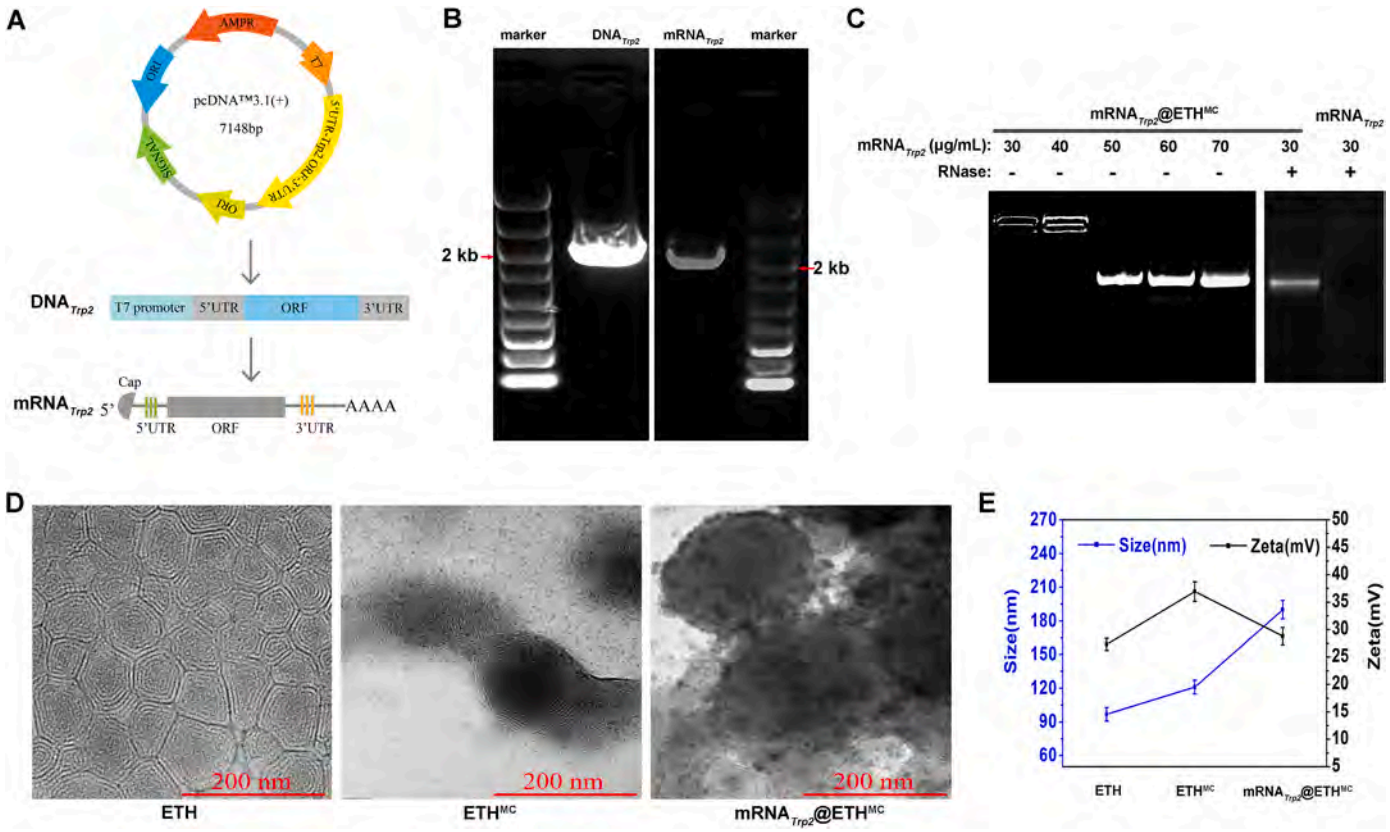

Fig. 1. Characterization of mRNA$_{Trp2}$@ETH^{MC}. (A) Schematic diagram of mRNA$_{Trp2}$ preparation process. (B) DNA$_{Trp2}$ and mRNA$_{Trp2}$ products were verified by agarose gel electrophoresis. (C) Gel retardation data to determine the optimal load of ETH^{MC} for RNAs and verify the ability of ETH^{MC} to protect mRNA from RNase. (D) Transmission electron microscopy images of ETH, ETH^{MC} and mRNA$_{Trp2}$@ETH^{MC}. (E) The particle potentials and sizes of ETH^{MC} and mRNA$_{Trp2}$@ETH^{MC} (Data are shown as means ± SD, n = 3).

as solvent. Aqueous solutions of $NaBH(OAc)_3$ (20 mM) and D-mannose (20 mM) were also prepared. Equal volumes of the three solutions were mixed by slowly stirring at room temperature for 48 h, followed by dialysis (MWCO 12–14 kDa) against deionized water for 72 h. Finally, the product was freeze-dried to obtain the MC.

2.3.2. Preparation of MC-modified ETH (ETH^{MC})

The ETH was synthesized by thin film dispersion as previously reported [17]. Briefly, Egg yolk lecithin, cholesterol and octadecylamine were mixed with a mass ratio of 50:5:2 and dissolved in 3 mL of ethanol by stirring. The solution was then transferred into a round-bottom flask and heated by water bath at a temperature of 40 °C, the ethanol was completely removed by rotary evaporation and a solid film was obtained at the bottom of the flask. Subsequently, 10 mL 30% ethanol containing mRNAs or siRNA$_{Pdl1}$ was added to rehydrate the film by stirring for 30 min at room temperature. The suspension product was then emulsified for 100 s at 80 W in an ice bath using a probe ultrasonic instrument (JY92-II, Ningbo Kechuang Biotechnology Co., Ltd., Ningbo, China). After filtering the emulsion multiple times with a 220 nm microporous membrane, ETH or RNAs-loaded ETHs with uniform particle size were obtained. To prepare ETH^{MC} loaded with IVT mRNAs or siRNA$_{Pdl1}$, the RNAs-loaded ETHs were mixed with an equal volume of 1 mg/mL hyaluronic acid (HA) aqueous solution and stirred slowly at room temperature for 2 h. Then, the mixture was centrifuged at 12,787×*g* for 10 min to remove free HA and added with 1% (w/v) MC acetic acid solution (pH = 4.0). After stirring and centrifugation with the same process, the empty Eth^{MC} or RNAs-loaded Eth^{MC} (mRNA$_{egfp}$@ETH^{MC}, mRNA$_{Trp2}$@ETH^{MC} or siRNA$_{Pdl1}$@ETH^{MC}) were obtained. DiI-labelled ETH and ETH^{MC} were also prepared for fluorescence microscopy. Briefly, 10 ml of ETH or ETH^{MC} solution were mixed with 0.2 mL of DiI, and then agitated for 30 min and dialyzed with ultrapure water for three days to obtain DiI-labelled ETH or ETH^{MC}. The morphology of ETHs was characterized by transmission electron microscopy (TEM, JEM-2100, Jeol Ltd., Tokyo, Japan) and the particle sizes and zeta potentials were measured by Zetasizer Nano ZS (ZEN3600, Malvern Panalytical Ltd., U.K.). ETH^{MC} was also characterized by Fourier-transform infrared (FTIR) spectroscopy with a FTIR spectrometer (Nicolet 6700, Thermo fisher, USA) in the range of 400–4000 cm^{-1}.

2.4. Gel retardation and RNase resistance assay

The optimal load of ETH^{MC} for RNAs was determined using agarose gel electrophoresis assay. ETH^{MC} loaded with different amount of mRNA was prepared, and the samples were evaluated by 1% agarose gel electrophoresis at 180 V for 15 min and imaged under UV light using a gel imager (FR-980B, Shanghai Furi Technology Co., Ltd., Shanghai, China). The ability of ETH^{MC} to protect IVT mRNA from degradation was also assessed in vitro with agarose gel electrophoresis. Briefly, the mRNA$_{Trp2}$@ETH^{MC} were treated with RNase for 1 h at room temperature, and the mixture was then incubated with EDTA for 10 min to inactivate RNase. Subsequently, 2% Triton X-100 was added to release mRNA, and the samples were analyzed with the same agarose gel electrophoresis described above.

2.5. Cytotoxicity assay

Cell viability was assessed by cell counting kit 8 and live/dead staining assays. DC2.4 cells were uniformly seeded in 24-well plates at 2 × 10^4 per/well and cultured in RPMI-1640 medium supplemented with 1% penicillin/streptomycin and 10% fetal bovine serum at 37 °C under

atmosphere of 5% CO_2 until the cell confluence reached about 80%. Then, the cells were treated with different concentrations of ETH or ETH^{MC} for 24 h. After washing with PBS for three times, each well was added 400 μL mixture of RPMI 1640 medium and CCK-8 reagent (at the ratio of 9:1) and incubated in the dark for 1 h. Subsequently, 100 μL supernatant was taken from each well and transferred to a 96-well plate, and the absorbance at 450 nm for each sample was measured using a microplate reader (1510, Thermo Fisher Scientific, Waltham, MA, USA). The cell viability was calculated according to equation (1). In addition, the above-treated cells were continued to co-incubate with 200 μl of 5 μM calcein-AM and 10 μM propidium iodide for 20 min in the dark. Finally, the morphology of the cells was observed and imaged with a fluorescence microscope (DMi 8, Leica Microsystems Ltd., Wetzlar, Germany).

$$\text{Cell viability} = \frac{\text{At} - \text{Ab}}{\text{Ac} - \text{Ab}} \times 100\% \quad (1)$$

At: absorbance of the tested samples; Ab: absorbance of the blank wells containing culture medium and CCK-8 solution but without cells; Ac: absorbance of the control.

2.6. Phagocytosis of ETH^{MC} by DCs in vitro

DC2.4 cells were seeded and cultured as described above. 100 μL DiI-labelled ETH or ETH^{MC} loading FITC was added and co-incubated with the cells for 4h, the cells treated with the equal volume of PBS or empty carriers were regarded as controls, followed by washing with PBS for three times. Then, the cells were fixed using 4% paraformaldehyde for 30 min and incubated with DAPI for 10 min, followed by washing with PBS for three times. Finally, the cells were visualized by a fluorescent microscope (DMi 8).

2.7. Transfection of DCs with $mRNA_{egfp}@ETH^{MC}$ in vitro

$mRNA_{egfp}$ was used as a model to transfect DCs in vitro to investigate whether mRNA-loaded ETH^{MC} can be successfully expressed in the cells. DC2.4 cells were seeded and cultured as described above. $mRNA_{egfp}@ETH^{MC}$ containing 2 μg $mRNA_{egfp}$ was added and co-incubated with the cells for 6 h in FBS-free RPMI-1640 medium. Then, the FBS-free medium was replaced with complete medium and continued to culture for 24 h, followed by observation using a fluorescence microscope (DMi 8).

2.8. Induction of DCs maturation by $mRNA_{Trp2}@ETH^{MC}$

DC2.4 cells were seeded into 6-well plates at 4×10^5 per/well and treated with $mRNA_{Trp2}@ETH^{MC}$, $mRNA_{Trp2}$/CpGs@ETH^{MC} or empty ETH^{MC} (2.5 μg/ml) for 24 h, and 2 μg of LPS or PBS were set as positive and negative control respectively. Cells were then digested by trypsin and washed with PBS for three times, and suspended in PBS at 1×10^6 cells/mL. Subsequently, 100 μL cell suspensions were taken and co-incubated with monoclonal antibodies of phycoerythrin-labelled goat anti-mouse CD80 and CD86 for 30 min at 4 °C. After washing with PBS for three times, the samples were resuspended in 300 μL PBS and examined by a flow cytometer (FACS Calibur, Becton Dickinson, Franklin Lakes, NJ, USA).

2.9. Test of knocking down PDL1 with $siRNA_{Pdl1}$ in vitro

DC2.4 cells were seeded and cultured as described above. Cells were treated with $siRNA_{Pdl1}$@ETHMC (2.5 μg/mL) or empty ETHMC for 24 h. Then, total RNAs were extracted from the cells and reverse transcribed to obtain cDNA using the reverse transcription kit. Subsequently, the obtained cDNA was used as template to run real time fluorescence quantitative PCR on a PCR machine (7500, Applied Biosystems Inc., Foster City, CA, USA) under the following conditions: denaturation at 95 °C for 2 min, followed by 40 cycles of 95 °C for 15 s and 62 °C for 32 s (primer sequences were shown in Table S1). The housekeeping gene *Gapdh* was used as an internal reference control and the relative level of $mRNA_{Pdl1}$ was calculated by the $2^{-\Delta\Delta Ct}$ method.

2.10. Preparation and characterization of transdermal patches

The sSFM was prepared with a facile immersion method based on the ternary solution reported previously [39]. Briefly, silkworm cocoon shells (SCS) were completely soaked in ternary solutions consisted of calcium chloride, ethanol and water in a mass ratio of 1:2:8 at 90 °C for overnight, followed by rinsing with 50% ethanol. sSFM was obtained after drying the rinsed samples for several hours in an oven at 60 °C. Microspheres containing drug-loaded ETH^{MC} were fabricated using a previously reported method. In details, 1g PVP was added to 6 mL of 60% ethanol solution, which was subsequently mixed with 4 mL vaccines ($mRNA_{Trp2}@ETH^{MC}$ and CpG@ETH^{MC} share the volume equally) or $siRNA_{Pdl1}@ETH^{MC}$ by stirring at room temperature. Then, the mixture was placed into 5 mL syringe to produce microspheres by electrospray under the following conditions: voltage 18 kV, receiving distance 15 cm, extrusion rate 1 mL/h, temperature 40 °C, humidity 8%. TCIP and TDSP were obtained by spraying microspheres loaded with vaccines or $siRNA_{Pdl1}@ETH^{MC}$ onto the sSFM, respectively.

The morphology of the patches was characterized by scanning electron microscopy (SEM, Phenom XL, Phenom Scientific, Shanghai, China). The mechanical properties of the patches were tested by a tensile testing machine (HY940-FS, Shanghai Hengyu Instrument Co., Ltd, China). The hydrophilicity and hydrophobicity of the patches was detected through the droplet angle measurement method using an Angle measuring instrument (DSA30 Kruss, Germany). The porosity of SFM was studied by the volume ratio method [34]. Briefly, the dried sSFM were cut into rectangle, measuring the length, width and thickness and calculating its volume and weight. Then the sSFM was immersed in an ethanol and weighed again. And the porosity was calculated according to equation (2). The moisture retention performance of the sSFM at 25 °C and 35% humidity was estimated by weighting the wet samples at different time points and calculated according to equation (3) [35].

$$\text{Porosity} = \frac{W_{ew} - W_d}{\rho_e \times V} \times 100\% \quad (2)$$

(Where W_d is the weight of dry sSFM, W_{ew} is the immediate weight of sSFM after soaking in ethanol, ρ_e is the density of ethanol).

$$\text{Moisturizing rate} = \frac{W_t - W_d}{W_w - W_d} \times 100\% \quad (3)$$

(Where W_d refers to the weight of dried sSFM, W_w is the immediate weight of sSFM after soaking in water, W_t is the weight of wet sSFM at time t).

2.11. Transdermal test in vitro

Skin permeation test in vitro was performed with Franz cells according to a previously-described method [16]. Briefly, the mouse skin samples were mounted separately on the diffusion cells with the epidermis facing up, and the drug-loaded patches covered the skin samples with the drug-loaded surface touching the stratum corneum. ETH^{MC} was labelled with DiI, and the linear DNA templates for in vitro transcription of TRP2 (termed as DNA_{Trp2}) were labelled with Hoechst 33342 and used as the model drugs encapsulated in ETH^{MC}. The receiving pool was filled with PBS buffer (pH = 7.4) and stirred continuously at 350 r/min while maintaining at 33 °C in a water bath. The experiment was run for 36 h and sampled at appropriate time intervals (2, 4, 6, 8, 10, 12, 24, 36 h). 2 ml receiving fluid were collected and immediately added with an equal volume of fresh PBS at each time point. The absorbance of the collected samples was measured at 354 nm by an ultraviolet spectrophotometer (TU-1810, Beijing Persee General

Instrument Co., Ltd., Shanghai, China), and the cumulative drug release against the skin was calculated according to equation (4).

$$Q = \frac{(\mathrm{VCn} + \sum_{i=1}^{n-1} \mathrm{C}i\mathrm{V}i)}{\mathrm{Q'}} \times 100\% \quad (4)$$

where Q is the cumulative amount of drug released, Q′ is the actual amount of drug contained in the Eths, V is the volume of the diffusion pool, C*i* is the drug concentration at *i* sampling time, and V*i* is the volume at *i* sampling time.

To measure the drugs remaining in the skin, the surface of the skin samples was washed with PBS for 3 times and then homogenized. 3 mL PBS was added and shook for 12 h in the dark. Subsequently, the mixture was centrifuged at 11988×*g* for 1 h and the absorbance value of the supernatants was measured at 354 nm using an ultraviolet spectrophotometer (TU-1810). The amount of drug retention in the skin was calculated according the same method above mentioned. To detect the drug distribution in the skin, the skin samples collected at the last time point were made into paraffin-embedded sections and observed using a fluorescence scanning imaging system.

2.12. Animal experiments

Five-week-old C57/BL6 male black mice were maintained in a 12 h light/dark cycle with free access to food and water (SPF environment). All animal experiments were performed under the guidelines approved by the Institutional Animal Care and Use Committee of Donghua University.

2.12.1. Detection of the TCIP-induced IgG and cytokines

The mice were anesthetized by intraperitoneal injection of 0.1 mL 1% pentobarbital solution. Then, the abdomen hair of each mouse was removed. After moistened the bare belly skin with PBS, the as-prepared TCIP (1.5 cm × 1.5 cm, the actual loading amounts for $mRNA_{Trp2}$ and CpGs were both 10 μg) was attached to the skin and fixed with medical tape for 3 days so that the patches can adhere closely to the skin. The same operation was repeated on the 7th and 14th day to boost the immunization. Non-administered mice served as control. Blood samples were collected from eye venous plexus (0.5 mL for each mouse) on days 3, 10 or 17, respectively. After standing for 30 min at RT, the blood samples were centrifuged for 5 min at 3000 rpm to obtain serum. Then, serum levels of TRP2 specific IgG, TNF-α, IFN-γ and IL-12 were determined by ELISA according to the manufacturer's protocol.

2.12.2. Evaluation of the anti-tumor effect of TCIP or/and TDSP

Mice were randomly divided into four groups (each with 4 mice): TCIP, TDSP, Combination treatment (TCIP + TDSP) and control. All the mice were inoculated with B16F10 cells (1×10^6/mouse) at the root of the thighs, and the day of inoculation was defined as day 0. For the groups receiving TCIP administration, mice were treated with TCIPs for three times, on days −21, −14 and −7 respectively following the same method described above. For the groups receiving TDSP administration, mice were treated with TDSP (1.5 cm × 1.5 cm, containing 10 μg $siRNA_{Pdl1}$) for four times, on days 5, 10, 15 and 20 respectively.

Tumor sizes as well as body weights were monitored every 2–3 days after inoculation of B16F10 cells. By measuring tumor length (L) and width (W), the volume (V) of tumor was calculated with equation (5). On day 23, the mice were sacrificed by cervical dislocation as the volume of tumors from control group were exceeding 2200 mm^3. Tumors, hearts, kidneys, livers, lungs and spleens were all removed and fixed in 4% paraformaldehyde solution. The tumor tissues were stained with terminal deoxynucleotidyl transferase-mediated dUTP nick-end labelling (TUNEL) and immunohistochemical staining of anti-CD4 and CD8 according to the instructions of the kits. In addition, paraffin sections of the tumors and viscera were prepared, stained with hematoxylin–eosin, observed and photographed under a microscope (DMi 8).

$$V = \frac{L \times W^2}{2} \quad (5)$$

2.13. Statistical analysis

All experiments were conducted at least three times, and numeric data were expressed as mean ± standard deviation (SD) unless otherwise indicated. Statistical significance was analyzed by one-way analysis of variance (ANOVA) with Tukey's post hoc test or unpaired *t*-test. A *p* value less than 0.05 was considered significant.

3. Results

3.1. Preparation and characterization of $mRNA_{TRP2}@ETH^{MC}$

DNA vector pcDNA™3.1(+) including T7 promoter, 5′UTR, ORF encoding TRP2 and 3′UTR in sequence was constructed and used as template for PCR to obtain DNA_{Trp2} (Fig. 1A & Fig. S1). DNA_{Trp2} was then used as template for production of $mRNA_{Trp2}$ and the expected size of $mRNA_{Trp2}$ is about 2000 bp, which was verified by electrophoresis assay (Fig. 1B).

Morphology of ETHs was characterized by TEM, which showed a multi-layer cystic spherical structure (Fig. 1D). The MC-modified ETH (ETH^{MC}) was successfully prepared as proved by FTIR spectra (Fig. S2). Compared to ETH, the size of ETH^{MC} increased from 97 nm to 121 nm due to the adsorption of HA and MC on the surface, and the potential of ETH^{MC} increased significantly due to the adsorption of MC (Fig. 1D&E). After drug loading, size of $mRNA_{Trp2}@ETH^{MC}$ had a greater increase compared with the empty ETH^{MC}, while the change of potential was the opposite due to the negatively charged mRNA (Fig. 1D&E). Cytotoxicity of ETH^{MC} was assessed by CCK and live/dead cell staining assays. According to the data (Fig. S3), ETH^{MC} showed no obvious cytotoxicity at the concentrations of no more than 30 μg/mL, which is consistent with previous reports [17]. In consideration of a balance between cytotoxicity and drug dosage, the concentration of ETH^{MC} in subsequent studies was set to 30 μg/mL.

The capacity of ETH^{MC} to encapsulate mRNA was determined by the gel retardation assay. As shown in Fig. 1C, migration of mRNA was completely blocked when the concentration of mRNA was no more than 40 μg/mL. At the concentration of 40 μg/mL, a bright band appeared in the sample well, indicating that RNA could not be completely enclosed and some of them were electrostatically adsorbed on the surface of the positively-charged Eth^{-MC}. To make the Eth^{-MC} enclose as much RNA as possible within its inner cavity through physical encapsulation, a concentration of 30 μg/mL for RNA was used in subsequent experiments. Fig. 1E also showed the electrophoresis of free $mRNA_{Trp2}$ and $mRNA_{Trp2}@ETH^{MC}$ (with the optimal loading) after being treated with RNase A and EDTA in turn. Obviously, the mRNA encapsulated in ETH^{MC} survived while the free mRNA was completely degraded by RNase, indicating that the coating of ETH^{MC} can protect mRNA from RNase attack. The stability of mRNA encapsulated in ETH^{MC} was also investigated by changing the storage time and temperature. As shown in (Fig. S4), with the protection of ETH^{MC}, mRNA was able to survival for at least three weeks at 4 °C.

3.2. Performance of ETH^{MC} on targeting DCs

The DCs-targeted performance of ETH^{MC} was evaluated by in vitro phagocytosis and fluorescence microscopy. As shown in Fig. 2, the uptake of ETH^{MC} by DCs was significantly more than that of ETH. FITC wrapped in ETH^{MC} also appeared in a large number of cells. These results are consistent with the previous report [36], confirming the good ability of ETH^{MC} to target DCs. The $mRNA_{egfp}$ was produced and used to assess the transfection efficiency of $mRNA_{egfp}@ETH^{MC}$ to DCs. As shown in Fig. S5, $mRNA_{egfp}$ was effectively transfected into DCs and expressed

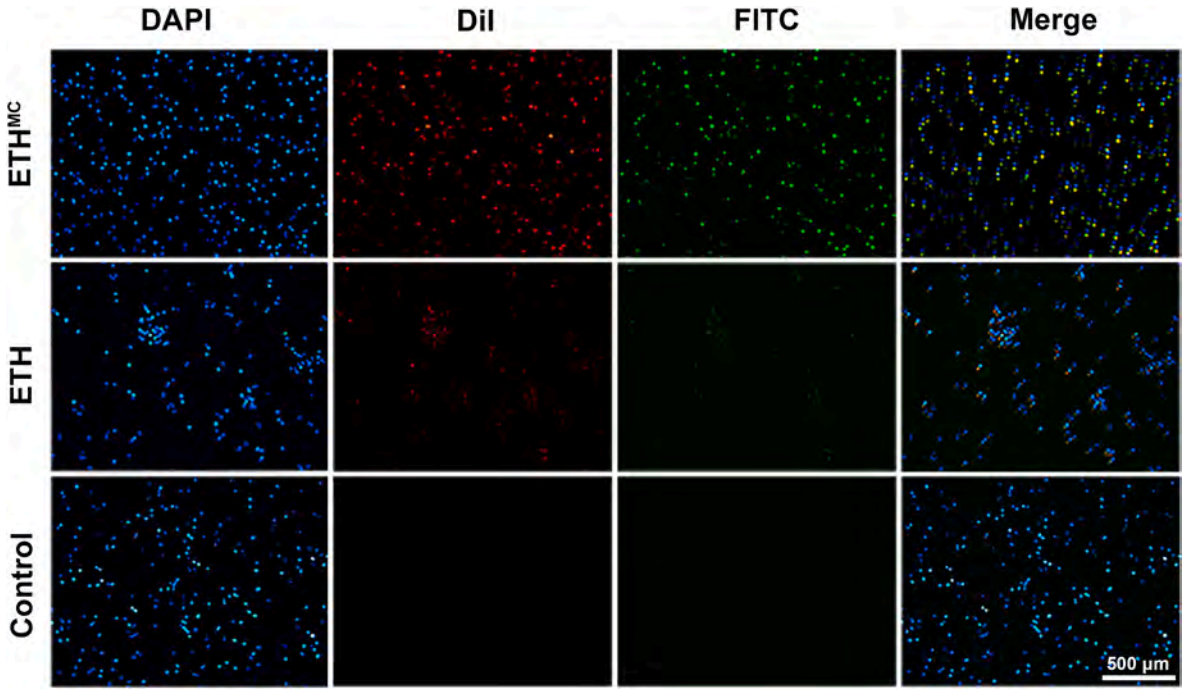

Fig. 2. Cellular uptake of ETH or ETH^{MC} by DCs (Blue fluorescence refers to nucleus stained by DAPI; Red fluorescence refers to ETH or ETH^{MC} labelled by DiI; Green fluorescence refers to FITC). (For interpretation of the references to colour in this figure legend, the reader is referred to the Web version of this article.)

normally. In addition, the transfection efficiency of mRNA encapsulated in ETH^{MC} was much higher than those in lipo8000 (a commercial transfection reagent) or ETH, which was consistent with the results in Fig. 2 and confirmed the good ability of ETH^{MC} to target DCs.

3.3. Performance of mRNA@ETH^{MC} on inducing DCs maturation in vitro

To investigate the ability of mRNA@ETH^{MC} to induce DCs maturation, the expression levels of CD80 and CD86 (two markers of the mature DCs) were detected after treating DCs with mRNA$_{Trp2}$@ETH^{MC} for 24 h in vitro. According to the flow cytometry data (Fig. 3A&B), mRNA$_{Trp2}$@ETH^{MC} significantly improved the expression levels of both CD80 and CD86, compared with the negative and positive controls. In addition, the combination of mRNA$_{Trp2}$@ETH^{MC} and CpG@ETH^{MC} showed a much stronger ability in promoting the expression of the markers than the single mRNA$_{Trp2}$@ETH^{MC} did. These results indicated that ETH^{MC} loaded with mRNA$_{Trp2}$ and CpG can effectively induce the maturation of DCs.

3.4. Morphology and transdermal performance of the patches

Microspheres composed of drug-loaded ETH^{MC} and PVP were sprayed onto the surface of the sSFM to obtain the transdermal patches. As shown in Fig. 4A, the sSFM had a porosity and loose structure made of uniform fibers, and the microspheres were evenly dispersed on the surface of the fibers. The porosity of sSFM is about 77.68% (Fig. S7A). Size of sSFM fibers and microspheres were 11 ± 2 μm and 683 ± 141 nm, respectively (Fig. 4B). Such a structure is conducive for the close adhesion of the drug-loaded microspheres to the skin and further promotes the transdermal delivery of drug. In addition, sSFM has a good tensile performance, which would not be affected by the introduction of microspheres (Fig. S7B). The moisturizing rate of sSFM for 24 h is about 45.37% at 25 °C and 35% humidity, showing a good moisture retention performance (Fig. S7C). The water contact angle of sSFM is about 81.46° and the angle is significantly reduced to 64.23° after its surface being sprayed with the microspheres (Fig. S7D), which indicates that sSFM is hydrophilic, and the attachment of microspheres improves its hydrophilicity.

The DNA$_{Trp2}$ labelled with Hoechst 33342 was used as the model drug to assess the transdermal performance of the patches by Franz diffusion method in vitro. As shown in Fig. 5A, the cumulative transdermal drug release over 36 h for the DNA$_{Trp2}$@ETH^{MC}-loaded patches was 35.4%, significantly higher than that for the control of free DNA$_{Trp2}$. The data of drug retention in the skin also showed a similar trend with the transdermal drug release (Fig. 5B&C). These results indicate that the prepared patches loaded with ETH^{MC} can effectively deliver nucleic acid molecules through transdermal route and the ETH^{MC} is helpful during the process.

3.5. Evaluation of immune activity of TCIP

Serum levels of TRP2-specific IgG and some immune related cytokines were detected by ELISA to evaluate the immune activity of TCIP. As shown in Fig. 6, the serum levels of IgG, TNF-α, IL-12 and IFN-γ of the mice administrated with TCIP were significantly higher than those of the untreated ones, and the levels increased with the increase of immunization times, suggesting that the transdermal administration of TCIP effectively elicited the immune response of mice.

3.6. Anti-tumor efficacy of TCIP or/and TDSP

Real-time fluorescence quantitative PCR was used to examine the effect of siRNA$_{Pdl1}$@ETH^{MC} lowering the expression of PDL1 in DCs. As shown in Fig. S6, mRNA level of PDL1 decreased significantly in the cells treated with siRNA$_{Pdl1}$-loaded carriers compared with the empty ETH^{MC}. Moreover, the cells treated with siRNA$_{Pdl1}$@ETH^{MC} expressed less PDL1 (about 20% of the control) than those with siRNA$_{Pdl1}$@Lipo8000 (about 33% of the control), which should be due to that ETH^{MC} is more efficient than Lipo8000 to transfect DCs, and also confirm the DCs-targeted ability of ETH^{MC}.

The anti-tumor activity of the TCIP or/and TDSP was evaluated using a syngeneic mouse model for melanoma. As shown in Fig. 7, the tumor volume in each group gradually increased with time, and the slowest tumor growth was in the group of combination treatment with TTVP and

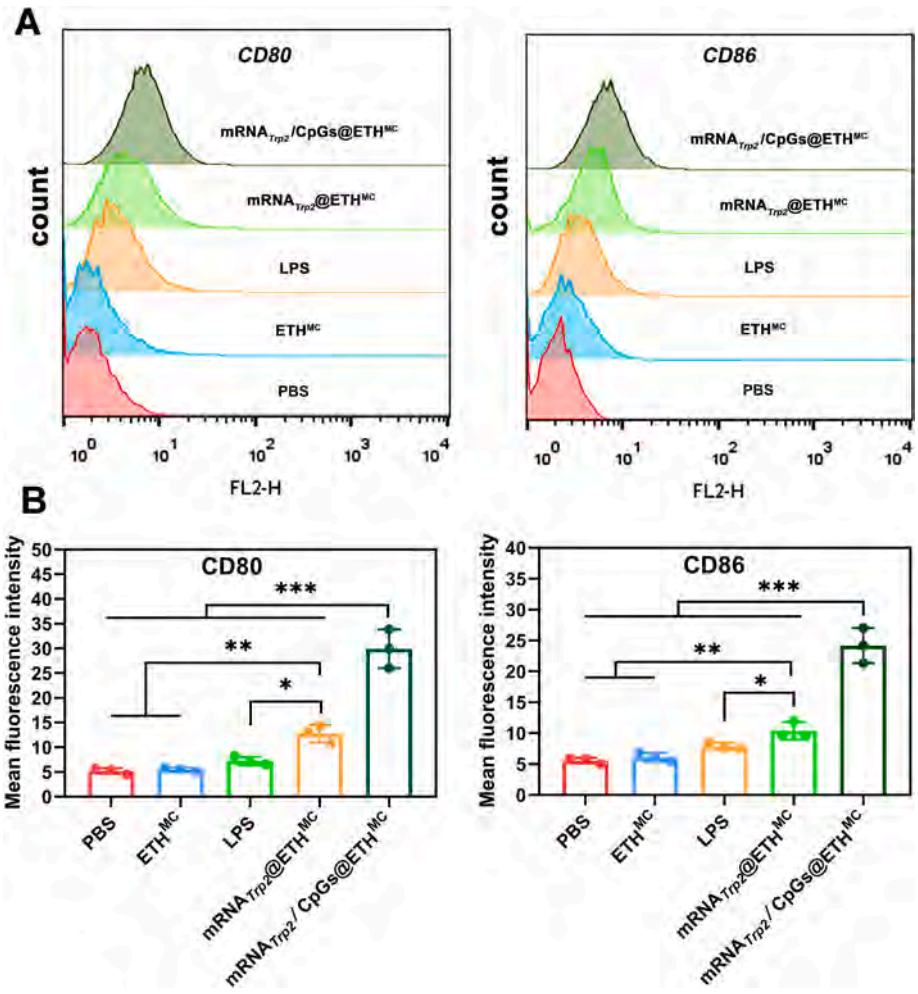

Fig. 3. Levels of CD80 and CD86 expressed by DCs treated with mRNA$_{Trp2}$/CpGs-loaded ETH^{MC} (A: Flow cytometry histograms of CD80 and CD86 expressed by DCs after different treatment; B: Quantitative analysis of B. Data are shown as means ± SD, n = 3; *$p < 0.05$, **$p < 0.01$, ***$p < 0.001$).

TDSP (Fig.7BD). The mice body weights increased over time with a trend similar to that of tumor growth, but no significant difference between the groups (Fig. 7C). There was significant difference in tumor volume and mass between the treatment groups and the control group, indicating that the treatments have significant antitumor effect (Fig.7BDEF). There were also difference among the different treatments, the combination treatment of TCIP and TDSP showed the strongest suppression on tumor growth, and the tumor suppression efficiency of TCIP single treatment was significantly higher than that of TDSP (Fig.7EF). The trend of survival rates (Fig. 7G) was similar with that of volumes (Fig. 7F). These results suggested that the administration with TCIP or/and TDSP can effectively inhibit the growth of tumor.

The tumor tissues were further investigated with H&E, TUNEL and immunohistochemistry staining (Fig. 8). As shown in Fig. 8 A&B, the treatment groups had much higher intensity of red fluorescence than the untreated control, indicating that the treatment with TCIP or/and TDSP improved the infiltration of $CD4^+$ and $CD8^+$ T cells in the tumor tissues. TUNEL staining results showed there were significantly more apoptotic cells (showing green fluorescence) in the treatment groups compared with the control. H&E staining results showed large areas of white and tan in the treatment groups, which represents the areas of necrosis due to the apoptosis of tumor cells. Moreover, there was significant difference in the $CD4^+/CD8^+$ T cells infiltration and tumor cells apoptosis between the different treatment groups, and the combination treatment with TCIP and TDSP exhibited the strongest ability to induce $CD4^+/CD8^+$ T cells infiltration and tumor cells apoptosis.

3.7. Biosafety evaluation of treatment with TCIP or/and TDSP

The heart, liver, spleen, lung and kidney of the treated mice was collected and stained with H&E for histopathological analysis to assess the biosafety of the treatment with TCIP or/and TDSP. As shown in Fig. 9, the cell structure of the organs is complete, morphology of the nuclear is normal and clear, and there was no cracking and shrinkage, suggesting no obvious pathology or local inflammation in the main organ and tissues after the treatment. Also, there is no significant difference between the treatment groups and the control. These results demonstrate that TCIP or/and TDSP treatments did not produce significant toxicity to the organs, suggesting the administration of TCIP or/and TDSP has a good biosafety.

4. Discussion

TCI represents an encouraging alternative to traditional vaccination approaches by overcoming their limitations such as invasive and pain, risk of infection or gastrointestinal irritation [40]. As a special type of liposome, ETH is capable to deliver drugs into deeper layers of the skin and increase their rate of transdermal absorption without any damage to the skin [41]. Our previous studies have proved that the modified ETHs with the ability to target DCs are useful vehicles for TCI, as they can effectively trigger antigen-specific immune responses via transcutaneous route [16,17]. The mRNA vaccines have attracted great attention in recent years for their advantages of avoiding the risk of DNA

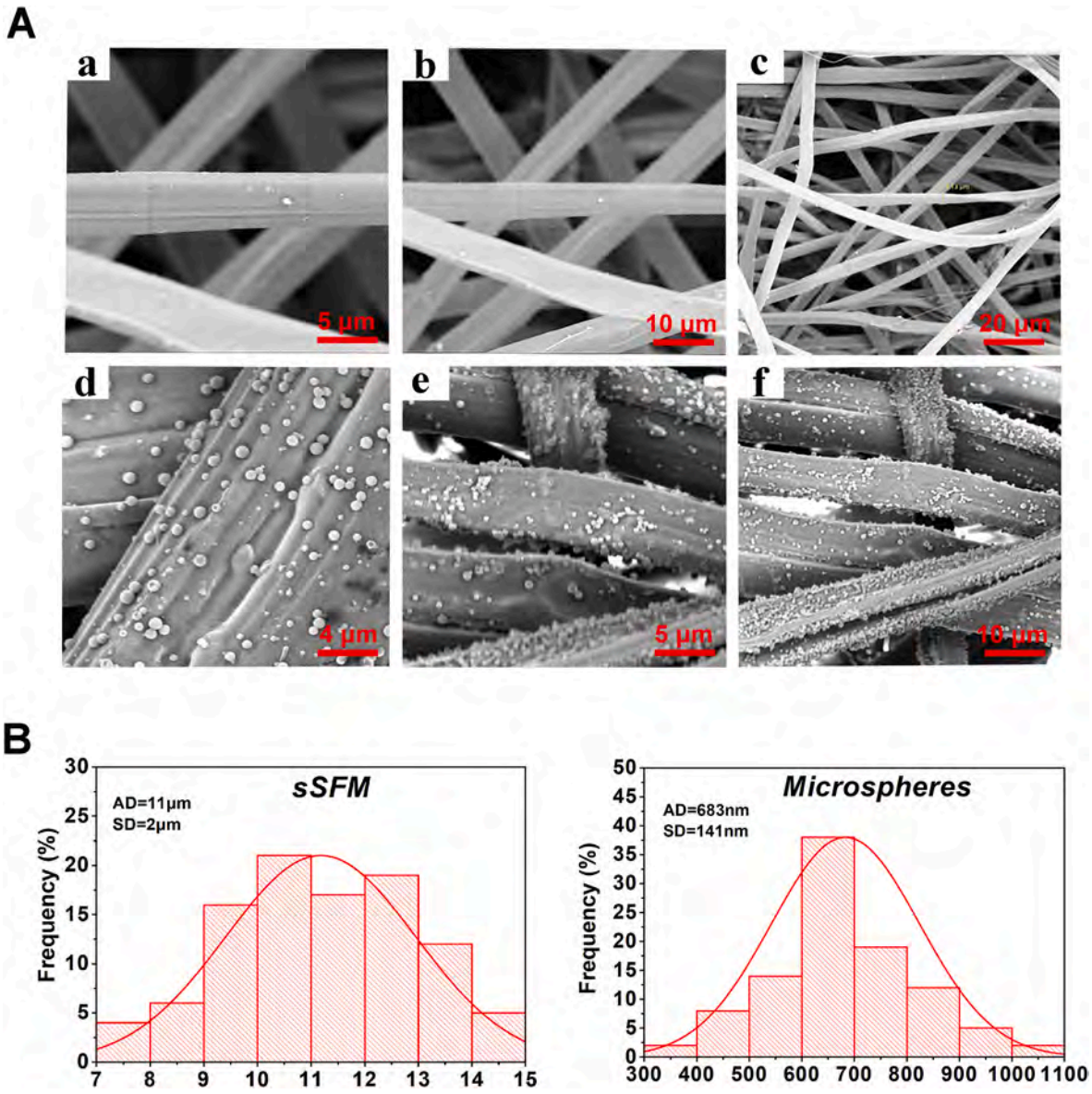

Fig. 4. Micrographs (A) and diameter distribution chart (B) of the transdermal patches (a–c: sSFM; d–f: transdermal patches).

contaminating the genome and the complicated expression and purification process required for protein antigens [42]. In this study, we aimed to deliver mRNA vaccines using such ETH-based TCI system, trying to integrate the unique advantages of both TCI and mRNA vaccines for a better application effect.

Since mRNA is easily degraded by RNase that is almost ubiquitous, the key to mRNA vaccines is how to ensure the stability of mRNA and its expression efficiency in cells. In the process of preparing IVT mRNA, in addition to the routine operation of using DEPC to treat all vessels, capping and tailing the transcripts with m7G and poly(A) are considered helpful to improve its stability [43,44]. Besides, the IVT mRNAs enveloped in nano-carriers such as lipid nanoparticles have been reported with good stability [45]. In addition, IVT mRNAs with appropriate 5′ UTR and 3′ UTR also have better stability and translation efficiency in cells [46,47]. Here, we proved that ETH encapsulation can protect the IVT mRNA from degradation by RNase (Fig. 1C), and mRNA stored in this way can survive for several weeks at a temperature of 4 °C (Fig. S4). With the modification of MC on the surface of ETH by electrostatic adsorption and layer by layer self-assembly, ETH^{MC} possessed a good ability to target DCs (Fig. 2). And ETH^{MC} showed a higher efficiency in transfecting DCs than lipo8000 (Fig. S5), which should be due to the DCs-targeted capacity of ETH^{MC}. The mRNA encapsulated in ETH^{MC} was successfully expressed after transfecting DCs (Fig. S5). Furthermore, $mRNA_{Trp2}$-loaded ETH^{MC} was observed to effectively induce DCs maturation in vitro (Fig. 3A&B). These results, coupled with its good transdermal performance (Fig. 5), demonstrated that ETH^{MC} is a suitable carrier for targeted delivery of mRNA vaccines to DCs through transcutaneous route.

For the convenience of use, the ETH^{MC} loaded with antigens and adjuvants was sprayed onto the fibrous substrates to produce TCIP by electrospraying, a facile method reported previously [17,19]. We used sSFM as the substrates, which can be obtained by simply soaking SCS in an eco-friendly ternary solution of $CaCl_2$-ethanol-H_2O. After soaking, the original compact SCS was changed into a loose sheet with fiber network structure (Fig. 4A). The sSFM has a good tensile performance (much better than that of eSFM as reported previously [19]) and moisture retention property (Fig. S7). These properties as well as the facile preparation method make sSFM a suitable base substrate for TDD patches. The microspheres containing drug-loaded ETH^{MC} were evenly distributed on the surface of sSFM (Fig. 4A), and the patches exhibited a good performance in delivering biomacromolecules into deep layer of the skin (Fig. 5). Therefore, the combination of ETH^{MC} and sSFM is a

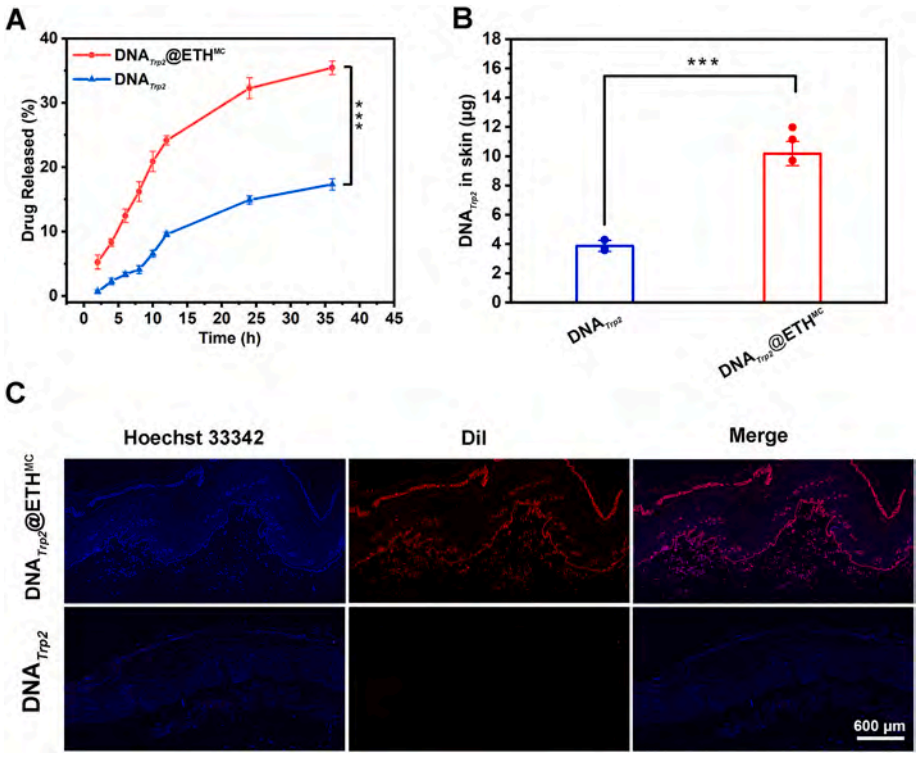

Fig. 5. ***In vitro*** **skin permeation data of the patches loaded with DNA$_{Trp2}$@ETH^{MC} or free DNA$_{Trp2}$** (A: Cumulative drug release curve; B: Drug retention in the skin; C: Fluorescence micrographs of skin sections after transdermal administration for 36 h (Red fluorescence: DiI-labelled ETH^{MC}; Blue fluorescence: DNA$_{Trp2}$ labelled with Hoechst 33342). Data in A and B are shown as means ± SD, n = 3; ***$p <$ 0.001). (For interpretation of the references to colour in this figure legend, the reader is referred to the Web version of this article.)

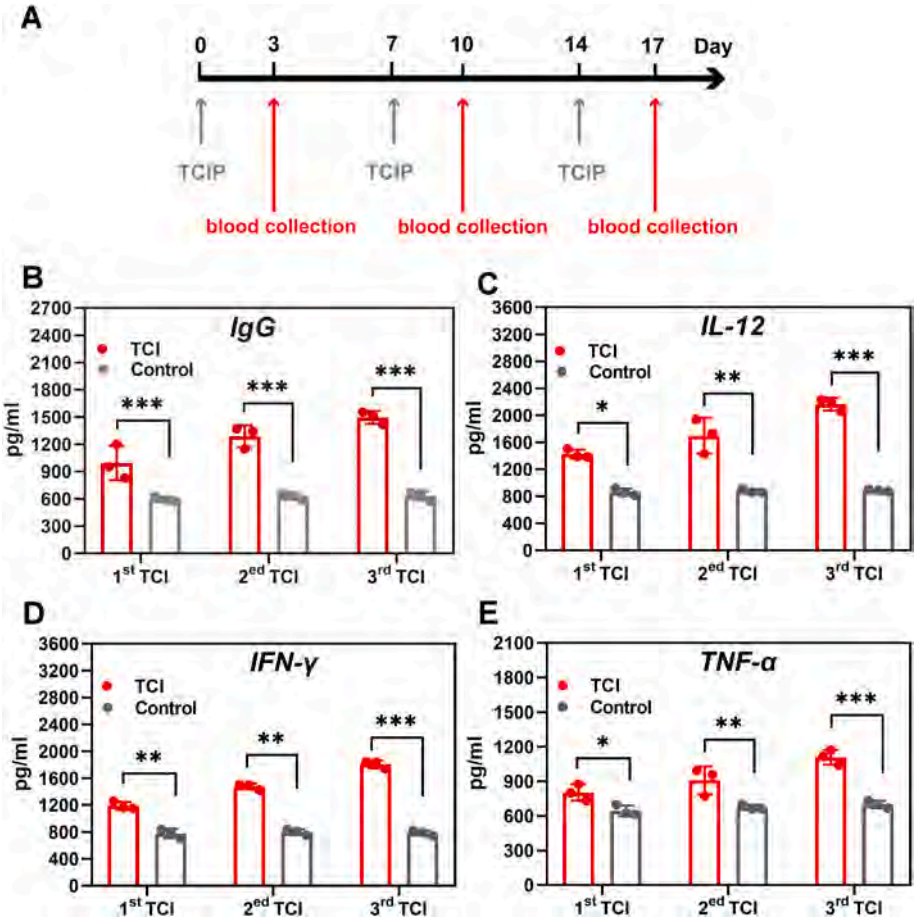

Fig. 6. Serum levels of TRP2-specific IgG and cytokines after administration with TCIP. (A) Schematic protocol of immunization and blood samples collection. (B) Levels of TRP2-specific IgG. (C) Levels of IL-12. (D) Levels of IFN-γ. (E) Levels of TNF-α. Data are shown as means ± SD, n = 3; *$p < 0.05$, **$p < 0.01$, ***$p < 0.001$.

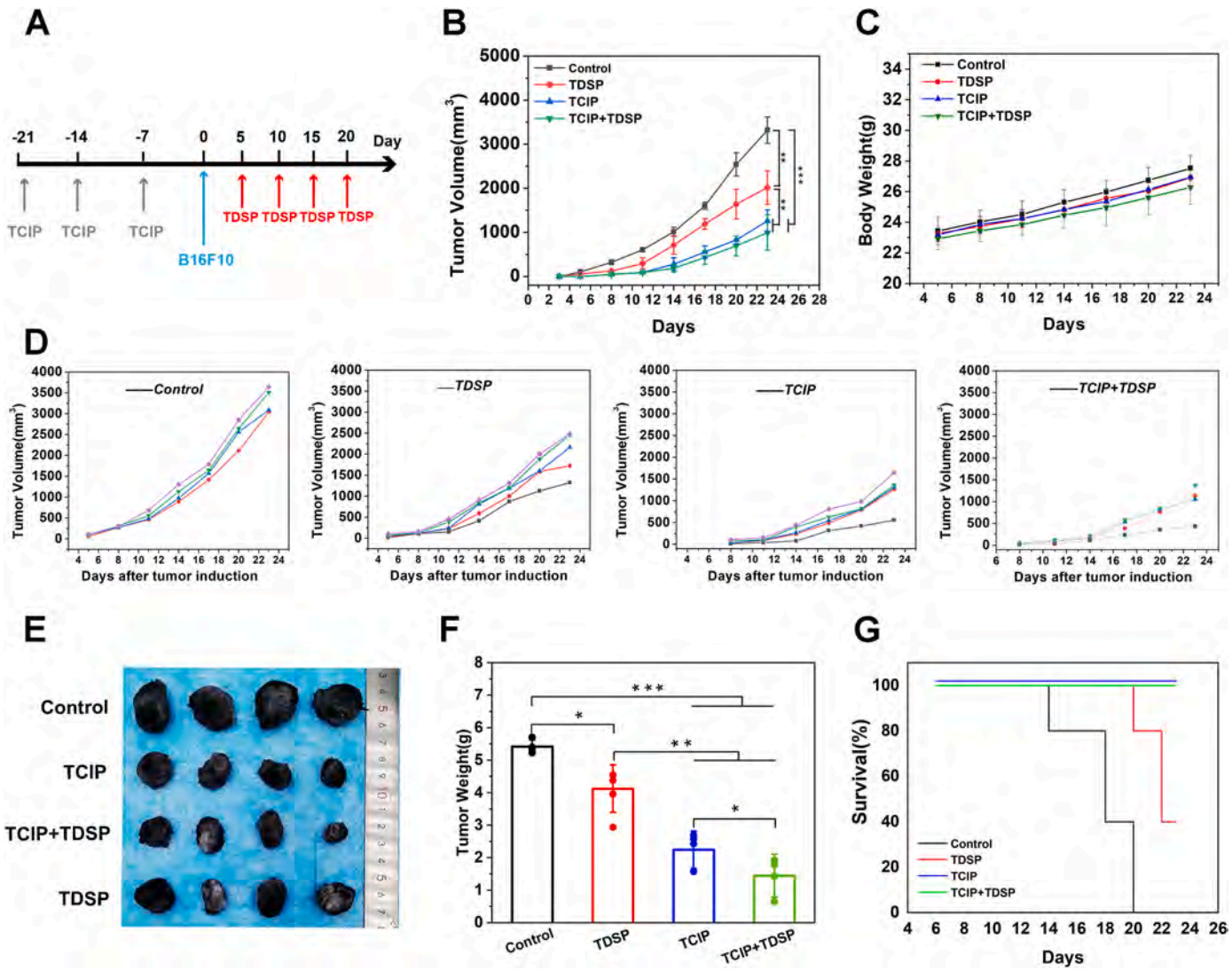

Fig. 7. Antitumor efficacy of different treatment in B16F10 Melanoma model. (A) Schematic protocol of *in vivo* antitumor experiments. (B) The average tumor growth curve. (C) Body weight of mice bearing tumor. (D) Individual mouse tumor growth curve. (E) Tumors isolated from the mice on day 23. (F) Tumor weight on day 23. (G) Survival rate (mice with a tumor volume exceeding 2000 mm^3 were considered dead). Data are shown as means ± SD, n = 4; $^*p < 0.05$, $^{**}p < 0.01$, $^{***}p < 0.001$.

good strategy for constructing patches for TCI or other treatments. The serum levels of TNF-α, IL-12, IFN-γ and TRP2-specific IgG were significantly increased after the administration of TCIP (Fig. 6), suggesting that the patches loaded with $mRNA_{Trp2}$@ETH^{MC} can effectively trigger TRP2-specific humoral and cellular immune responses. Thus, the feasibility and effectiveness of the above TCI system to deliver mRNA vaccine was also confirmed *in vivo*.

Immunotherapy has attracted extensive attention in recent years, including tumor vaccines, ICB and chimeric antigen receptor T-cells [48]. It can eliminate tumor cells by stimulating the patient's own immune system and has the advantages of high efficiency, low toxicity and not easy to relapse compared with traditional therapies [49]. Many studies have shown that the combination of multiple means, such as tumor vaccine combined with ICB, can achieve better tumor suppression effects [50]. The high efficiency, noninvasive and convenience of TCI provide a broad space for its application, and some progress has been made in percutaneous delivery of tumor vaccine for anti-tumor application [16,17,19,51]. Knockdown of PDL1 expression with siRNA has been chosen by more researchers as an immune checkpoint blocking strategy, because it can avoid the risk of immune system hyperactivity caused by blocking PD1 [24]. We have reported that transdermal delivery of tumor vaccine or cytokines to DCs using ETH can effectively inhibit tumor growth [16,17,19]. Moreover, the combination of TCI and aPD1 can further improve the anti-tumor effect compared with the TCI or aPD1 monotherapies [17,19]. In this study, we tried for the first time to use a similar TCI system to deliver mRNA vaccines and anti-PDL1 siRNA for the treatment of tumor. Using mouse melanoma as a model, TCIP and TDSP were applyed to the skin before and after tumor inoculation, respectively. The results showed that the application of TCIP or/and TDSP can significantly inhibit the growth of melanoma (Fig. 7). Moreover, a large number of $CD4^+$ and $CD8^+$ T cells infiltrated in the tumor tissue after treatment (Fig. 8). The massive infiltration of $CD4^+$ and $CD8^+$ T cells as well as the high expression of cytokines (TNF-α, IL-12, IFN-γ) may be important reasons for the apoptosis of tumor cells, as these cytokines are the key indicators of robust anti-tumor immune response [52]. However, the antitumor effect of TDSP in this study was significantly weaker than TCIP, which may be because: 1) The dose of $siRNA_{Pdl1}$ contained in TDSP was not enough to significantly knock down the level of PDL1 *in vivo*; 2) TDSPs were attached to the abdomen of mice in this study, and it may be more effective to administer them to the tumor site. The analysis of tissue sections of important organs such as heart, liver, lung, kidney and spleen suggest that the administration of

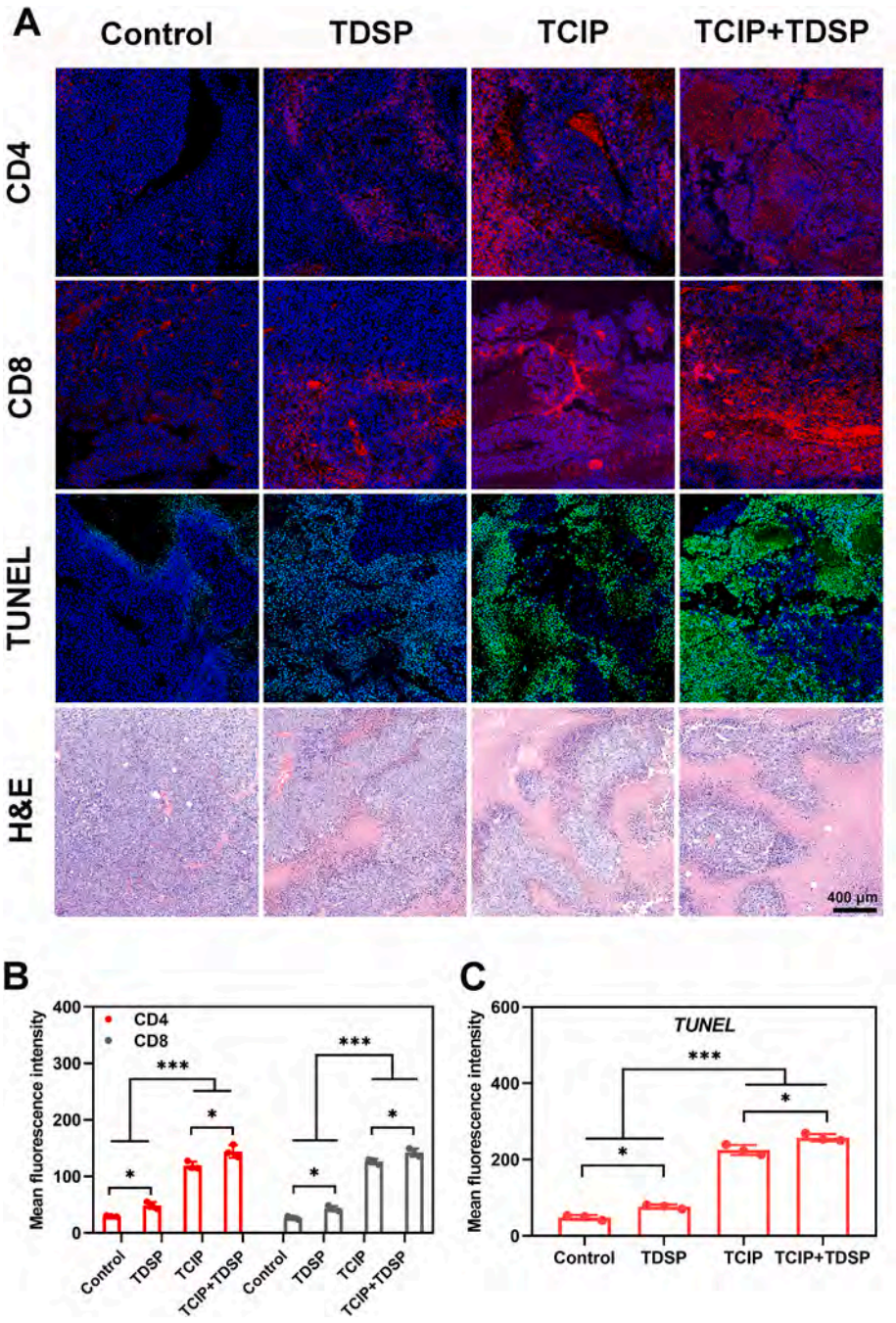

Fig. 8. Micrographs of tumor tissues stained by H&E, TUNEL and antibodies of CD4 or CD8 (A), fluorescent intensity of CD4 and CD8 (B) and TUNEL staining (C) (Data are expressed as mean ± SD, n = 3; *$p < 0.05$, ***$p < 0.001$).

TCIP or/and TDSP have good biosafety.

The anti-tumor strategy of tumor vaccine combined with ICB shows good results. Most previous studies used this combined treatment strategy after tumor vaccination. However, the main function of vaccine is prevention, although tumor vaccine has been proved to have therapeutic effect. Therefore, it is valuable to explore the application strategy of combining the prophylactic activity of tumor vaccine with the therapeutic effect of ICB. Herein, we adopted such a strategy, that is, applying TCIP before tumor inoculation coupled with TDSP after tumor inoculation. Our data shows that this combined treatment has a better antitumor effect than the monotherapy groups did (Figss. 8and 9). Interestingly, it has been reported recently that the combination of tumor vaccines and ICB has significant prophylactic activity against tumors [14,19]. It would be meaningful to compare the antitumor activity of different application modes of combination treatment with tumor vaccines and ICB.

To our knowledge, this study is the first attempt to use ETH-based TCI system for delivery of mRNA vaccines and anti-PDL1 siRNA for tumor immunotherapy. Our data proved the feasibility and effectiveness of this novel strategy. We believe that there is still much room to improve the efficacy of this strategy by optimizing the technical details, which is expected to have a better effect in tumor immunotherapy.

5. Conclusion

In this study, the feasibility of transcutaneous delivery of mRNA vaccine via patches based on ETH^{MC}/sSFM was investigated. The results showed that ETH^{MC} is a good carrier for DCs-targeted delivery of mRNA

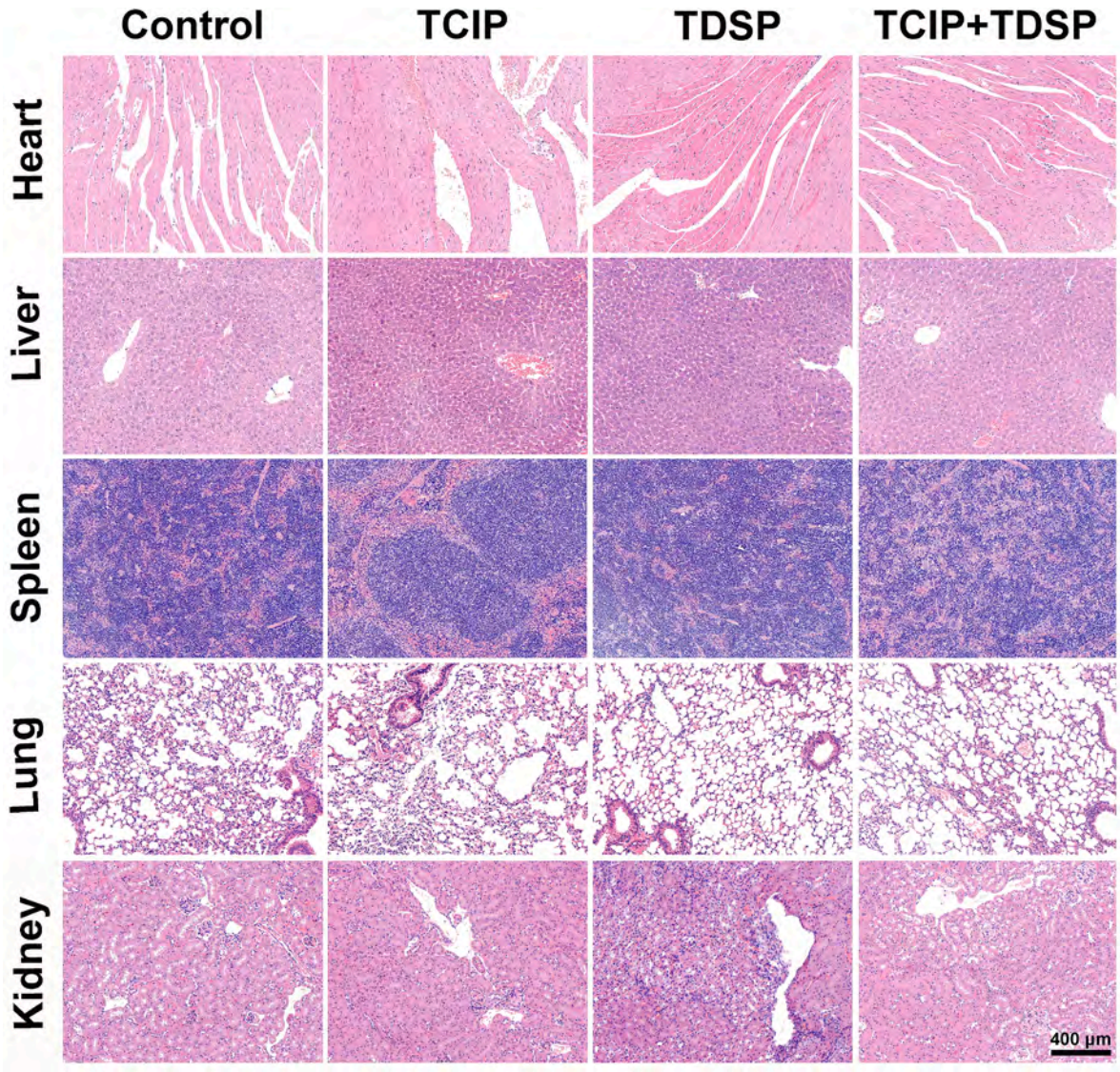

Fig. 9. Micrographs of H&E-stained tissue sections of major organs from the melanoma-bearing mice after different treatment.

through transdermal route, since it has good performances in targeting DCs and protecting mRNA from being degraded by RNase as well as good transdermal ability. Animal experiments using mouse melanoma as a model demonstrated the prophylactic activities of TCIP on inhibiting tumor growth by delivering mRNA vaccines. And the application of TDSP delivering anti-PDL1 siRNA was also shown significantly suppressing the growth of tumor. The combination of TCIP and TDSP showed a better ability to promote $CD4^+/CD8^+$ T cells infiltration in tumor tissues and induce tumor cells apoptosis. Considering the advantages of efficiency, non-invasiveness and convenience, the strategy of TCIP combined with TDSP has good application potential in tumor immunotherapy.

6. Credit authorship contribution statement

Kaili Wang: Conceptualization, Methodology, Investigation, Writing-original draft. Xiaoyun Wang: Conceptualization, Methodology, Funding acquisition. Di Jiang: Methodology, Validation. Yifei Pei: Investigation. Zhe Wang: Investigation. Xiaojun Zhou: Methodology. Jinglei Wu: Methodology. Xiumei Mo: Conceptualization. Hongsheng Wang: Conceptualization, Methodology, Investigation, Writing-editing, Funding acquisition. Supervision.

Declaration of competing interest

The authors declare that they have no known competing financial interests or personal relationships that could have appeared to influence the work reported in this paper.

Acknowledgements

This research was supported by Science and Technology Commission of Shanghai Municipality (18490740400, 20DZ2254900), the National Key Research and Development Program of China (2018YFC1706200) and Science & Technology Committee of Songjiang District, Shanghai (2020SJ361).

Appendix A. Supplementary data

Supplementary data to this article can be found online at https://doi.org/10.1016/j.compositesb.2022.109648.

References

[1] Chen Z, Lv Y, Qi J, et al. Overcoming or circumventing the stratum corneum barrier for efficient transcutaneous immunization. Drug Discov Today 2018;23(1):181–6.

[2] Pielenhofer J, Sohl J, Windbergs M, et al. Current progress in particle-based systems for transdermal vaccine delivery. Front Immunol 2020;11:266.
[3] Belyakov IM, Hammond SA, Ahlers JD, et al. Transcutaneous immunization induces mucosal CTLs and protective immunity by migration of primed skin dendritic cells. J Clin Invest 2004;113(7):998–1007.
[4] Kaurav M, Minz S, Sahu K, et al. Nanoparticulate mediated transcutaneous immunization: myth or reality. Nanomedicine 2016;12(4):1063–81.
[5] Karande P, Mitragotri S. Transcutaneous immunization: an overview of advantages, disease targets, vaccines, and delivery technologies. Annu Rev Chem Biomol Eng 2010;1:175–201.
[6] Sallam MA, Prakash S, Kumbhojkar N, et al. Formulation-based approaches for dermal delivery of vaccines and therapeutic nucleic acids: recent advances and future perspectives. Bioeng Trans Med 2021;6(3):e10215.
[7] Saliba H, Heurtault B, Bouharoun-Tayoun H, et al. Enhancing tumor specific immune responses by transcutaneous vaccination. Expert Rev Vaccines 2017;16 (11):1079–94.
[8] Chen M, Yang D, Sun Y, et al. In situ self-assembly nanomicelle microneedles for enhanced photoimmunotherapy via autophagy regulation strategy. ACS Nano 2021;15(2):3387–401.
[9] Xu J, Xu B, Tao J, et al. Microneedle-assisted, DC-targeted Codelivery of pTRP-2 and adjuvant of paclitaxel for transcutaneous immunotherapy13; 2017. p. 1700666. 28.
[10] Kim NW, Kim SY, Lee JE, et al. Enhanced cancer vaccination by in situ nanomicelle-generating dissolving microneedles. ACS Nano 2018;12(10):9702–13.
[11] Wu A, Chen Y, Wang H, et al. Genetically-engineered "all-in-one" vaccine platform for cancer immunotherapy. Acta Pharm Sin B 2021;11(11):3622–35.
[12] Wang C, Ye Y, Hochu GM, et al. Enhanced cancer immunotherapy by microneedle patch-assisted delivery of anti-PD1 antibody. Nano Lett 2016;16(4):2334–40.
[13] Wakabayashi R, Kono H, Kozaka S, et al. Transcutaneous codelivery of tumor antigen and resiquimod in solid-in-oil nanodispersions promotes antitumor immunity. ACS Biomater Sci Eng 2019;5(5):2297–306.
[14] Rausch J, Lopez PA, Bialojan A, et al. Combined immunotherapy: CTLA-4 blockade potentiates anti-tumor response induced by transcutaneous immunization. J Dermatol Sci 2017;87(3):300–6.
[15] Pandey V, Golhani D, Shukla R. Ethosomes: versatile vesicular carriers for efficient transdermal delivery of therapeutic agents. Drug Deliv 2015;22(8):988–1002.
[16] Yang X, Wang X, Hong H, et al. Galactosylated chitosan-modified ethosomes combined with silk fibroin nanofibers is useful in transcutaneous immunization. J Contr Release 2020;327:88–99.
[17] Hong H, Wang X, Song X, et al. Transdermal delivery of interleukin-12 gene targeting dendritic cells enhances the anti-tumour effect of programmed cell death protein 1 monoclonal antibody. Biomater Transl 2021;2(2):151–64.
[18] Le Moignic A, Malard V, Benvegnu T, et al. Preclinical evaluation of mRNA trimannosylated lipopolyplexes as therapeutic cancer vaccines targeting dendritic cells. J Contr Release 2018;278:110–21.
[19] Song X, Hong H, Fawal GE, et al. Transcutaneous tumor vaccination combined with aPD-1 treatment produces a synergistic antitumor effect. Acta Biomater 2021. https://doi.org/10.1016/j.actbio.2021.11.033.
[20] Mayoux M, Roller A, Pulko V, et al. Dendritic cells dictate responses to PD-L1 blockade cancer immunotherapy. Sci Transl Med 2020;12(534):eaav7431.
[21] Daneshmandi S, Pourfathollah AA, Karimi MH, et al. PDL-1/PDL-2 blockade in mice dendritic cells by RNAi techniques to induce antitumor immunity. Immunotherapy 2015;7(11):1145–58.
[22] Wang Y, Zhang L, Xu Z, et al. mRNA vaccine with antigen-specific checkpoint blockade induces an enhanced immune response against established melanoma. Mol Ther 2018;26(2):420–34.
[23] Pillai RN, Behera M, Owonikoko TK, et al. Comparison of the toxicity profile of PD-1 versus PD-L1 inhibitors in non-small cell lung cancer: a systematic analysis of the literature. Cancer 2018;124(2):271–7.
[24] Chaudhri A, Xiao Y, Klee AN, et al. PD-L1 binds to B7-1 only in cis on the same cell surface. Cancer Immunol Res 2018;6(8):921–9.
[25] Pardi N, Hogan MJ, Porter FW, et al. mRNA vaccines - a new era in vaccinology. Nat Rev Drug Discov 2018;17(4):261–79.
[26] Schlake T, Thess A, Fotin-Mleczek M, et al. Developing mRNA-vaccine technologies. RNA Biol 2012;9(11):1319–30.
[27] Kallen KJ, Thess A. A development that may evolve into a revolution in medicine: mRNA as the basis for novel, nucleotide-based vaccines and drugs. Ther Adv Vaccines 2014;2(1):10–31.
[28] Mockey M, Bourseau E, Chandrashekhar V, et al. mRNA-based cancer vaccine: prevention of B16 melanoma progression and metastasis by systemic injection of MART1 mRNA histidylated lipopolyplexes. Cancer Gene Ther 2007;14(9):802–14.
[29] Kowalski PS, Rudra A, Miao L, et al. Delivering the messenger: advances in technologies for therapeutic mRNA delivery. Mol Ther 2019;27(4):710–28.
[30] Fan L, Li JL, Cai Z, et al. Bioactive hierarchical silk fibers created by bioinspired self-assembly. Nat Commun 2021;12(1):2375.
[31] Fan L, Li JL, Cai Z, et al. Creating biomimetic anisotropic architectures with Co-aligned nanofibers and macrochannels by manipulating ice crystallization. ACS Nano 2018;12(6):5780–90.
[32] Yang X, Fan L, Ma L, et al. Green electrospun Manuka honey/silk fibroin fibrous matrices as potential wound dressing. Mater Des 2017;119:76–84.
[33] Wang Q, Zhou S, Wang L, et al. Bioactive silk fibroin scaffold with nanoarchitecture for wound healing. Compos B Eng 2021;224:109165.
[34] Yan S, Han G, Wang Q, et al. Directed assembly of robust and biocompatible silk fibroin/hyaluronic acid composite hydrogels. Compos B Eng 2019;176:107204.
[35] Hu Z, Das SK, Yan S, et al. Stability and biodegradation of silk fibroin/hyaluronic acid nerve conduits. Compos B Eng 2020;200:108222.
[36] Hong H, Zhang D, Lin S, et al. Green electrospun silk fibroin nanofibers loaded with cationic ethosomes for transdermal drug delivery. Chem Res Chin Univ 2021;37(3): 488–95.
[37] Ma L, Wang X, Wu J, et al. Polyethylenimine and sodium cholate-modified ethosomes complex as multidrug carriers for the treatment of melanoma through transdermal delivery14; 2019. p. 2395–408. 18.
[38] Martín-Alfonso JE, Číková E, Omastová M. Development and characterization of composite fibers based on tragacanth gum and polyvinylpyrrolidone. Compos B Eng 2019;169:79–87.
[39] Yang C, Shang S, Shou D, et al. Transforming natural silk nonwovens into robust bioadhesives for in vivo tissue amendment. J Clean Prod 2021;314:127996.
[40] Gupta Prem N, Vyas Suresh P. Colloidal carrier systems for transcutaneous immunization. Curr Drug Targets 2011;12(4):579–97.
[41] Carita AC, Eloy JO, Chorilli M, et al. Recent advances and perspectives in liposomes for cutaneous drug delivery. Curr Med Chem 2018;25(5):606–35.
[42] Liu MA. A comparison of plasmid DNA and mRNA as vaccine technologies. Vaccines (Basel) 2019;7(2):37.
[43] Fan YN, Li M, Luo YL, et al. Cationic lipid-assisted nanoparticles for delivery of mRNA cancer vaccine. Biomater Sci 2018;6(11):3009–18.
[44] Yamamoto A, Kormann M, Rosenecker J, et al. Current prospects for mRNA gene delivery. Eur J Pharm Biopharm 2009;71(3):484–9.
[45] Oberli MA, Reichmuth AM, Dorkin JR, et al. Lipid nanoparticle assisted mRNA delivery for potent cancer immunotherapy. Nano Lett 2017;17(3):1326–35.
[46] Lee K, Kim TS, Seo Y, et al. Combined hybrid structure of siRNA tailed IVT mRNA (ChriST mRNA) for enhancing DC maturation and subsequent anticancer T cell immunity. J Contr Release 2020;327:225–34.
[47] Youn H, Chung JK. Modified mRNA as an alternative to plasmid DNA (pDNA) for transcript replacement and vaccination therapy. Expet Opin Biol Ther 2015;15(9): 1337–48.
[48] Daassi D, Mahoney KM, Freeman GJ. The importance of exosomal PDL1 in tumour immune evasion. Nat Rev Immunol 2020;20(4):209–15.
[49] Zheng DW, Gao F, Cheng Q, et al. A vaccine-based nanosystem for initiating innate immunity and improving tumor immunotherapy. Nat Commun 2020;11(1):1985.
[50] Sahin U, Oehm P, Derhovanessian E, et al. An RNA vaccine drives immunity in checkpoint-inhibitor-treated melanoma. Nature 2020;585(7823):107–12.
[51] Ye Y, Wang C, Zhang X, et al. A melanin-mediated cancer immunotherapy patch. Sci Immunol 2017;2(17):eaan5692.
[52] Li L, Yu R, Cai T, et al. Effects of immune cells and cytokines on inflammation and immunosuppression in the tumor microenvironment. Int Immunopharm 2020;88: 106939.